

Contents lists available at ScienceDirect

Climate Services

journal homepage: www.elsevier.com/locate/cliser





New projections of 21st century climate and hydrology for Alaska and Hawai'i

Naoki Mizukami ^{a,*}, Andrew J. Newman ^a, Jeremy S. Littell ^b, Thomas W. Giambelluca ^c, Andrew W. Wood ^a, Ethan D. Gutmann ^a, Joseph J. Hamman ^{a,d}, Diana R. Gergel ^e, Bart Nijssen ^f, Martyn P. Clark ^g, Jeffrey R. Arnold ^{h,i}

- ^a National Center for Atmospheric Research, Boulder, CO, USA
- ^b U.S. Geological Survey Alaska Climate Adaptation Science Center, Anchorage, AK, USA
- ^c University of Hawaiʻi at Manoa, Department of Geography, Honolulu, HI, USA
- d CarbonPlan, San Francisco, CA, USA
- e BlackRock, USA
- f University of Washington, Civil and Environmental Engineering, Seattle, WA, USA
- g Centre for Hydrology, University of Saskatchewan, Canmore, AB, Canada
- ^h U.S. Army Corps of Engineers, Responses to Climate Change Program, Seattle, WA, USA
- i Now at MITRE Corporation, McLean, VA, USA

ARTICLE INFO

Keywords: Hydrology Climate Projections Ensembles Alaska Hawai'i

ABSTRACT

In the United States, high-resolution, century-long, hydroclimate projection datasets have been developed for water resources planning, focusing on the contiguous United States (CONUS) domain. However, there are few statewide hydroclimate projection datasets available for Alaska and Hawai'i. The limited information on hydroclimatic change motivates developing hydrologic scenarios from 1950 to 2099 using climate-hydrology impact modeling chains consisting of multiple statistically downscaled climate projections as input to hydrologic model simulations for both states. We adopt an approach similar to the previous CONUS hydrologic assessments where: 1) we select the outputs from ten global climate models (GCM) from the Coupled Model Intercomparison Project Phase 5 with Representative Concentration Pathways 4.5 and 8.5; 2) we perform statistical downscaling to generate climate input data for hydrologic models (12-km grid-spacing for Alaska and 1km for Hawai'i); and 3) we perform process-based hydrologic model simulations. For Alaska, we have advanced the hydrologic model configuration from CONUS by using the full water-energy balance computation, frozen soils and a simple glacier model. The simulations show that robust warming and increases in precipitation produce runoff increases for most of Alaska, with runoff reductions in the currently glacierized areas in Southeast Alaska. For Hawai'i, we produce the projections at high resolution (1 km) which highlight high spatial variability of climate variables across the state, and a large spread of runoff across the GCMs is driven by a large precipitation spread across the GCMs. Our new ensemble datasets assist with state-wide climate adaptation and other water planning.

Introduction

Hydroclimate projection assessments are typically motivated by the need to evaluate potential societal impacts of climate change, including security of local/regional water resources. In the United States, federal and non-federal institutions, including the Bureau of Reclamation, US Army Corps of Engineers, and research institutes, have performed several hydroclimate projection studies for the contiguous United States

(CONUS) domain. That work has produced a large archive of high-resolution (~10-km or less), century long, CONUS-domain, hydro-climatologic projection products using off-line process-based hydrologic models forced by downscaled Global Climate Model (GCM) outputs (Maurer et al. 2013; Reclamation 2011, 2013, 2014, 2020; Kao et al. 2016). The deliberate attention to the main sources of uncertainty in climate projections (i.e., using multiple emission scenarios, and multiple GCMs; Hawkins and Sutton, 2009) enabled simulating a wide range of

E-mail address: mizukami@ucar.edu (N. Mizukami).

https://doi.org/10.1016/j.cliser.2022.100312

^{*} Corresponding author.

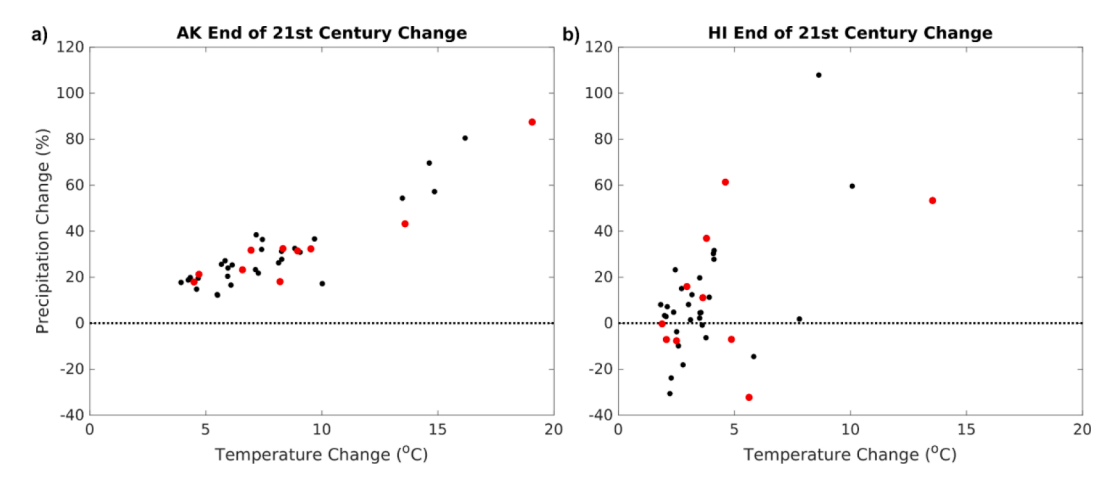


Fig. 1. a) Alaska and b) Hawai'i annual precipitation change (%) versus temperature (°C) change for the late-century period (2070–2099) under RCP8.5. Dots represent 40 CMIP5 GCMs. GCMs selected for downscaling are highlighted in red and listed in Table 1.

hydrologic projection outcomes, which can be used by local, regional, and national stakeholders in water resources adaptation planning structured around risk framing (e.g., Terando et al. 2020).

While a few studies have performed hydrologic projection simulations using sub-regional or basin-specific modeling within Alaska (Hay and McCabe 2010) and Hawai'i (Safeeq and Fares 2012; Mair, 2019), no domain-wide hydroclimate projections similar to the CONUS domain products existed for Alaska and Hawai'i. Lacking such products, stakeholders in both states often rely on any studies available that derive simple water balance simulations (e.g., Abatzoglou et al. 2018), but do not incorporate dynamic hydrologic simulations tailored to their regions. Both states have unique landscapes and hydroclimatic regimes that require scientifically motivated and specialized modeling considerations. For example, in Alaska, hydrologic processes are influenced by cryospheric processes such as permafrost, glaciers, as well as seasonal snowpack (Hinzman et al. 2005), while Hawai'i exhibits highly spatially varying meteorological fields, influenced by the trade wind pattern and islands' orography (Giambelluca et al. 2013; Xue et al., 2020).

Here we generate an ensemble of century-long hydroclimate projections for Alaska and Hawai'i that expands on Variable Infiltration Capacity (VIC; Liang et al. 1994) model-based hydrologic projections for CONUS by representing additional hydrologic processes (in our Alaska application) or by representing the domain at high spatial resolution (in our Hawai'i application). In doing so, we address a need for climate and hydrology projection datasets for Alaska and Hawai'i. Our approach uses a consistent methodology. For both regions, we compiled ten GCM climate outputs from phase 5 of the Coupled Model Intercomparison Project (CMIP5) for two emission scenario pathways (RCP 4.5 and RCP 8.5). These GCM outputs were then spatially downscaled using the Bias Corrected Spatial Disaggregation statistical downscaling method (BCSD; Wood et al. 2004). Finally, we produce hydrologic outputs using the VIC model forced by each downscaled climate scenario.

While we use the same VIC hydrologic model for both regions, we configure the VIC model to incorporate the modeled representations of several land surface processes unique to the arctic environment in Alaska. These include: 1) freeze—thaw of soil moisture based on the full energy balance; 2) organic soil content that affects subsurface hydraulic and thermal conductivity; and 3) a simple glacier model (Hamman, 2015; see section 3.2.1). We also adapt a glacier spin-up methodology to the VIC glacier model in an effort to provide realistic initial glacier states for the VIC simulations. The results of the Alaska simulations highlight some of the important hydrologic model components that will be required in order to properly simulate the dominant hydrological processes and their future changes in arctic environments around the world. For Hawai'i, we use the same VIC model physics configuration as the CMIP5 CONUS domain studies (Reclamation 2014, 2020). Because of

Table 1List of the 10 GCMs selected from the CMIP5 archive including the specific ensemble member and model resolution.

GCM Name	Ensemble Member	GCM Resolution		
ACCESS1-3	r1i1p1	$1.875 \times 1.25^{\circ}$		
CCSM4	r6i1p1	$0.942 \times 1.25^{\circ}$		
CSIRO-Mk3-6-0	r1i1p1	$1.865 \times 1.875^{\circ}$		
CanESM2	r1i1p1	$2.791 \times 2.813^{\circ}$		
GFDL-ESM2M	r1i1p1	$2.023 \times 2.5^{\circ}$		
HadGEM2-ES	r1i1p1	$1.25\times1.875^{\circ}$		
INM-CM4	r1i1p1	$1.5 imes 2^{\circ}$		
MIROC5	r1i1p1	$1.401 \times 1.406^{\circ}$		
MPI-ESM-MR	r1i1p1	$1.865 \times 1.875^{\circ}$		
MRI-CGCM3	rlilp1	$1.121 \times 1.125^{\circ}$		

high spatial variability of precipitation within each island, however, we use $1\ \mathrm{km}$ for the model spatial resolution.

In this paper, we detail the modeling approaches, the results on hydroclimatic change for both regions, and information on dataset availability. The remainder of the paper is structured as follows. In Section 2 we describe the methods used, including GCM selection, downscaling, and hydrologic model configurations specific to each domain. In Section 3 we describe the downscaled climatology and hydrologic projections focused on the middle and end of the 21st century. In Section 4 we describe known limitations to these outputs by region. Finally, in Section 5, we provide our conclusions.

Methods

GCM selection

Fig. 1 shows plots of the percent change in annual precipitation against change in temperature at the end of this century under RCP8.5, projected by 40 CMIP5 GCMs used in previous hydroclimate projection studies over CONUS (Reclamation, 2013, 2020). The GCM selection process considers several factors that affect variation in simulated climate futures primarily focused on capturing the spread of the CMIP5 projections while selecting a diverse set of GCMs to account for model structural diversity. The 10 GCM simulations, sub-selected from these 40 are from different models and modeling centers, are highlighted in red in Fig. 1 and listed in Table 1. They generally capture the domain-wide average spread of the entire 40 ensemble members for both domains, but not necessarily all the diverse responses across small subregions (Section 3.1). The specific ensemble member selected for each GCM (Table 1) follows previous CONUS hydroclimate projection work (Reclamation, 2013, 2020). We use two future concentration pathways

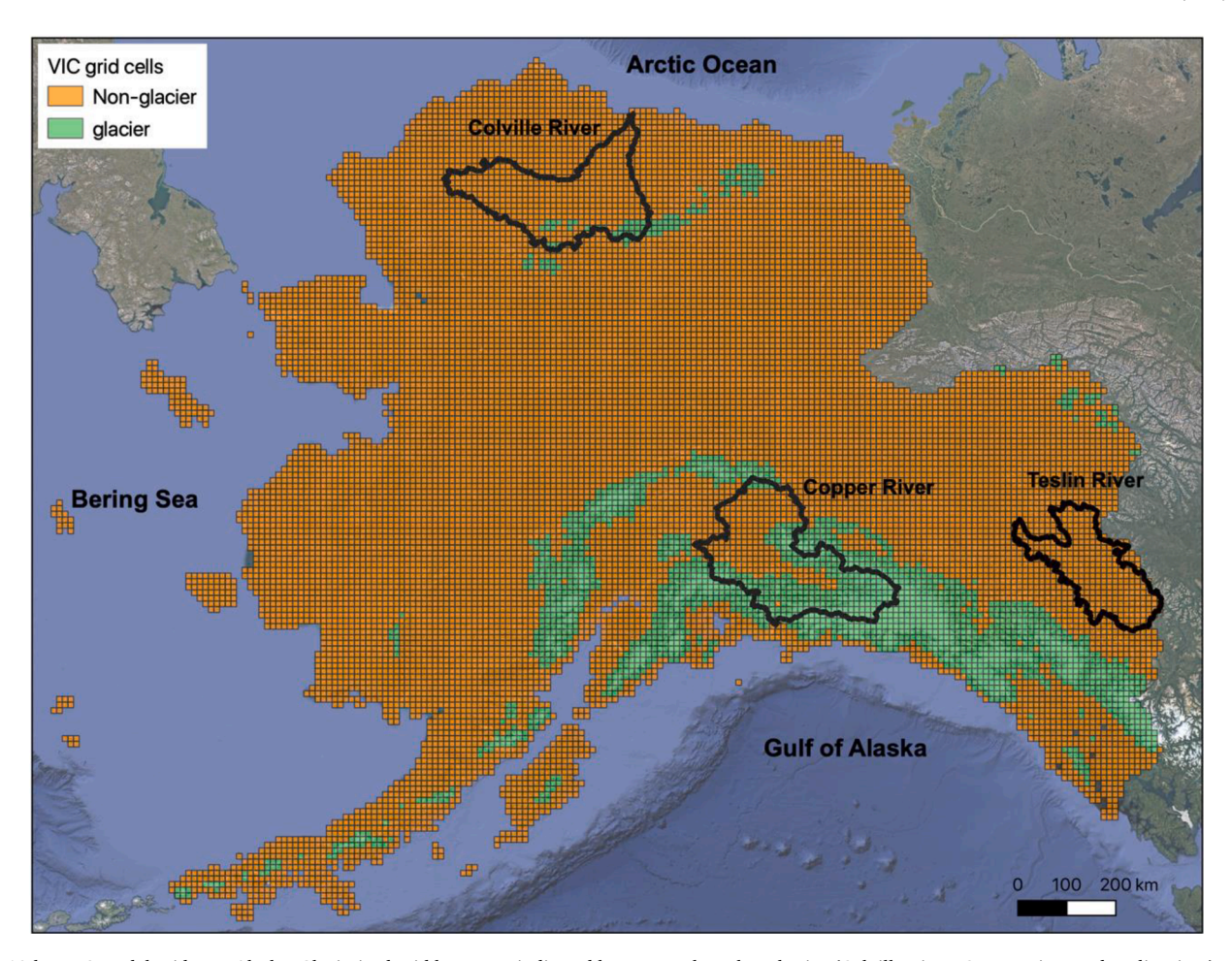


Fig. 2. 12-km VIC model grid over Alaska. Glacierized grid boxes are indicated by green color. Three basins (Colville River, Copper River and Teslin River) are used for Fig. 8.

for our projections: RCP4.5 and RCP8.5. All models show Alaska to be warmer and wetter in the future over nearly the entire domain for both RCPs (Figs. S6-AK to S9-AK). For Hawai'i, absolute changes are warming over the entire state for both RCPs, with an ensemble mean statewide drying for RCP4.5 and an ensemble mean wetting for RCP8.5 (Figs. S6-HI to S9-HI). While most models project wetting over Hawai'i, some project drying and we include both possibilities within our projections (Fig. 1b). GCM evaluation and selection is a topic of active research and discussion across the climate modeling and impact analysis communities with a wide array of methods available. In particular, the newest ideas are focusing on the need for application specific evaluation methodologies while still including scientifically justifiable evaluation metrics (Baumberger et al. 2017; Parker, 2020), which could include emergent constraints (e.g., Simpson et al. 2021; Williamson et al., 2021), global and regional scale change metrics (e.g., global temperature trends) (Tokarska et al. 2020), process-oriented metrics, and extremes (e.g. Newman et al. 2022).

Downscaling method

We use one statistical downscaling (SD) method—BCSD (Wood et al. 2004)— to generate daily downscaled precipitation and air temperature (daily minimum and maximum). BCSD is a computationally inexpensive method that can be applied to a large ensemble of GCM outputs over a large domain for improved characterization of uncertainty, while reproducing observed precipitation characteristics (such as wet-day frequency, extreme event) with better or similar fidelity compared to several other SD methods (Gutmann et al. 2014; Reclamation 2020).

BCSD has been widely used in the water resources climate impacts modeling community. For example, BCSD was used in the past two Bureau of Reclamation sponsored CONUS CMIP-based hydrologic projection studies (Reclamation 2011, 2013, 2014). With downscaled daily precipitation and air temperature, other meteorological variables (i.e., shortwave radiation, longwave radiation and humidity) are estimated at the high-resolution using Mountain Microclimate Simulation Model (MTCLIM; Thornton and Running 1999) algorithm. Such high-resolution radiation and humidity variables are consistent with precipitation and temperature as the MTCLIM algorithm accounts for cloudiness based on the occurrence of precipitation to estimate incoming radiation and for diurnal temperature range to estimate humidity.

We apply BCSD as it was initially designed in Wood et al. (2004). BCSD begins with bias correcting monthly mean GCM output at its original resolution based on a spatially aggregated, gridded observational dataset (coarsened observational grid to match the GCM grid). The bias correction in BCSD uses an empirical quantile mapping method (Panofsky and Brier, 1968) which corrects quantiles in the GCM cumulative distribution to the observational distribution. BCSD then performs a bi-linear interpolation to spatially disaggregate both the biascorrected GCM output and the coarsened observational data to the original high-resolution observational grid. Differences between the original observational dataset and the spatially disaggregated coarsened observational dataset are used to impose high resolution spatial variability on the spatially disaggregated GCM output. Finally, temporal disaggregation of the monthly downscaled GCM data is performed by first randomly selecting a daily sequence of a given month from the historical period (e.g., a future July monthly precipitation would be disaggregated using a randomly selected historical July daily sequence), then scaling (precipitation) or shifting (for temperature) the selected daily sequence so that monthly means of the adjusted daily series match the downscaled monthly GCM values. The BCSD technique has been extensively used and tested so that its characteristics are generally well known and not recreated here. Downscaled climate data using BCSD represent historical monthly values and seasonality very well, have better spatial scaling and representation of interannual variability than other methods, and maintain features of ENSO spatial correlation patterns in the original large-scale model (e.g. Gutmann et al. 2014; Sun et al. 2020).

A key decision when applying BCSD (or any other statistical downscaling method) is selecting the high-resolution observational product which is used to train the downscaling method. For Alaska, we use a 12km gridded dataset for the period 1980-2017, which is aggregated from the 1-km Daymet dataset version 3 (Thornton et al. 2016). For Hawai'i we use a 1-km gridded dataset for the period 1990-2013, which is aggregated from the 250-m dataset recently developed by the University of Hawai'i (Longman et al. 2019). The length of observed data is different between the two regions (37 years for Hawai'i and 23 years for Hawai'i), and is shorter than the 50-year record used for CONUS hydroclimate projection work (Reclamation 2013). With a shorter length observational dataset, the uncertainty in extreme events in the downscaled product may become greater because the short observation record length increases the uncertainty in the tails (extreme events) of the observed cumulative distribution used for quantile mapping based bias correction (Wood et al., 2004).

Hydrologic modeling

As was done in the CMIP5-based CONUS hydroclimate projection studies (Reclamation 2014, 2020), we use the VIC hydrologic model for both Alaska and Hawai'i to produce daily hydrologic variables from 1950 through 2099. In this study we used version 4.2.glacier, versus version 4.1.2 (Reclamation 2014) and version 4.2.c (Reclamation 2020). For both regions, we estimated VIC soil parameters based on publicly available global geophysical datasets: Soil textural data from SoilGrids (250 m resolution; Hengl et al. 2016) and topography data from the Advanced SpaceBorne Thermal Emission Radiometer-Global Digital Elevation Model Version 2 (30 m resolution; ASTER-GDEM2; Tachikawa et al. 2011), along with the transfer functions (i.e., functions to convert geophysical properties to model parameters) defined by Mizukami et al. (2017). Mizukami et al. (2017) calibrated the parameters of the transfer function that compute VIC soil parameters using the streamflow observations at the CAMELS (Catchment Attributes and Meteorology for Large-sample Studies; Addor et al., 2017) basins over CONUS. VIC vegetation parameters, including roughness and resistance, are assigned to each land cover type using a vegetation library. In VIC, the other vegetation parameters-monthly climatological Leaf Area Index (LAI) and Albedo— can either be assigned to each land cover type in the library or each grid box independently from land cover type. Below, we describe model configurations and parameters specific to each region.

Alaska

Fig. 2 shows the VIC simulation domain at 12-km resolution over Alaska. The VIC configuration includes several model specifications that represent the processes in the arctic environment. First, we use VIC's frozen soil algorithm (Cherkauer and Lettenmaier 1999) to simulate soil freeze—thaw based on computed soil temperature. With the frozen soil mode turned on, surface energy and moisture fluxes are numerically solved by minimizing energy and water balance errors. The frozen soil mode requires a sub-daily computational time step to resolve the diurnal cycle of energy fluxes; here, we use a 2-hr time step. Second, Alaska, like other arctic regions, is rich in soil organic matter that affects soil hydraulic and thermal properties (Lawrence and Slater 2008). Therefore, we use Soil Carbon Content (g/kg) data from SoilGrids to estimate the

soil organic matter to adjust soil hydraulic conductivity and thermal conductivity. Lastly, we use the simple glacier model implemented in VIC (Hamman, 2015) to simulate separate snow and ice accumulation and ablation. The glacier model simulates ice accumulation, withinpixel ice redistribution, and ablation, but does not move glacier across neighboring pixels. The glacier model converts a portion of snowpack into ice when the predicted snowpack density becomes greater than a threshold value (700 kg/m³). Then, the computed ice volume is converted to an ice cover area using the area-volume relationship of Bahr (1997). During the glacier area computation, the glacier is distributed from the highest elevation to lower elevation bands within the single grid box. Here, we define sub-grid elevation bands at a grid box if the elevation relief within the grid box exceeds 500 m based on ASTER-GDEM2 elevation data. Each band is defined such that the mean elevation of each band is equally spaced. The number of elevation bands depends on the sub-grid elevation range, but is limited to five. The subgrid elevation bands also account for elevational effects on temperature, which affect snow and ice accumulation and melt. Finally, the ice layer is integrated into the snowpack layer to compute the energy balance and the corresponding ice and snow melt. The glacier model was run for 1,913 grid boxes (out of a total of 14,227 12-km grid boxes) as shown in Fig. 2. The glacier grid boxes are determined based on the Randolph Glacier Inventory v6.0 (RGI v6.0; Pfeffer et al. 2014). More specifically, any 12-kim grid boxes that overlap glacier polygons in the RGI image are considered as glacier grid boxes.

VIC vegetation parameters are based on the land-cover dataset recently developed for the VIC model application for arctic regions (Gergel 2019). This land cover dataset uses 0.05-degree resolution Plant Functional Types (PFTs) implemented in the Community Land Model (CLM) 4.5, which include 17 unique plant types that distinguish optical properties, stomatal physiology, roughness length, displacement height, and so on; therefore represents unique energy and water exchanges such as snow interaction and evapotranspiration. Unique VIC vegetation parameters except for LAI and albedo are assigned to each PFT. Monthly LAI and surface albedo used are also based on the CLM4.5 input dataset, which is generated independently from the PFT.

Model initialization is performed in two steps: first glacier initialization, followed by initialization of the remaining energy and moisture states. For glacier initialization (performed only for glacier pixels), we first apply the area-volume scaling relationship of Bahr (1997) to each glacier extent obtained from the RGI v6.0 dataset to estimate the ice volume for each glacier extent. The ice volume is then distributed to each VIC grid box based on the grid box area fraction of the total glacier extent. Finally, the ice volume is converted to areal average ice thickness, which is used as the initial ice thickness in the VIC glacier model. Since the extent of almost all RGI glaciers over Alaska is based on the satellite images taken during the period between 2000 and 2011, the estimated ice volume from RGI glacier extent needs to be adjusted to better represent the glacier volumes in 1950. Assuming the RGI glacier extent represents the extent in the year of 2000, glacier ice volume reconstruction was made via iterative VIC simulations from 1950 to 2000, starting with initial guess of ice thickness in 1950, which is updated at each iteration based on ice thickness error in the year of 2000 from the previous VIC run. The VIC runs for the glacier initialization use one of the downscaled GCMs, CCSM4, instead of initialization for each GCM because the glacier initialization has a high computational cost and the downscaled historical climates from all 10 GCMs are very similar as a result of the bias correction applied (shown in Fig. S1-AK through S5-AK in supplement materials).

Once a glacier is initialized, a 5-year (1950–1954) simulation is cycled five times for each downscaled GCM forcing. The visual inspection confirms soil hydraulic and thermal states are stabilized after the VIC model spin-up. During this spin up process, the glacier ice thickness is initialized at each spin-up iteration to the ice thickness estimated via the glacier initialization process.

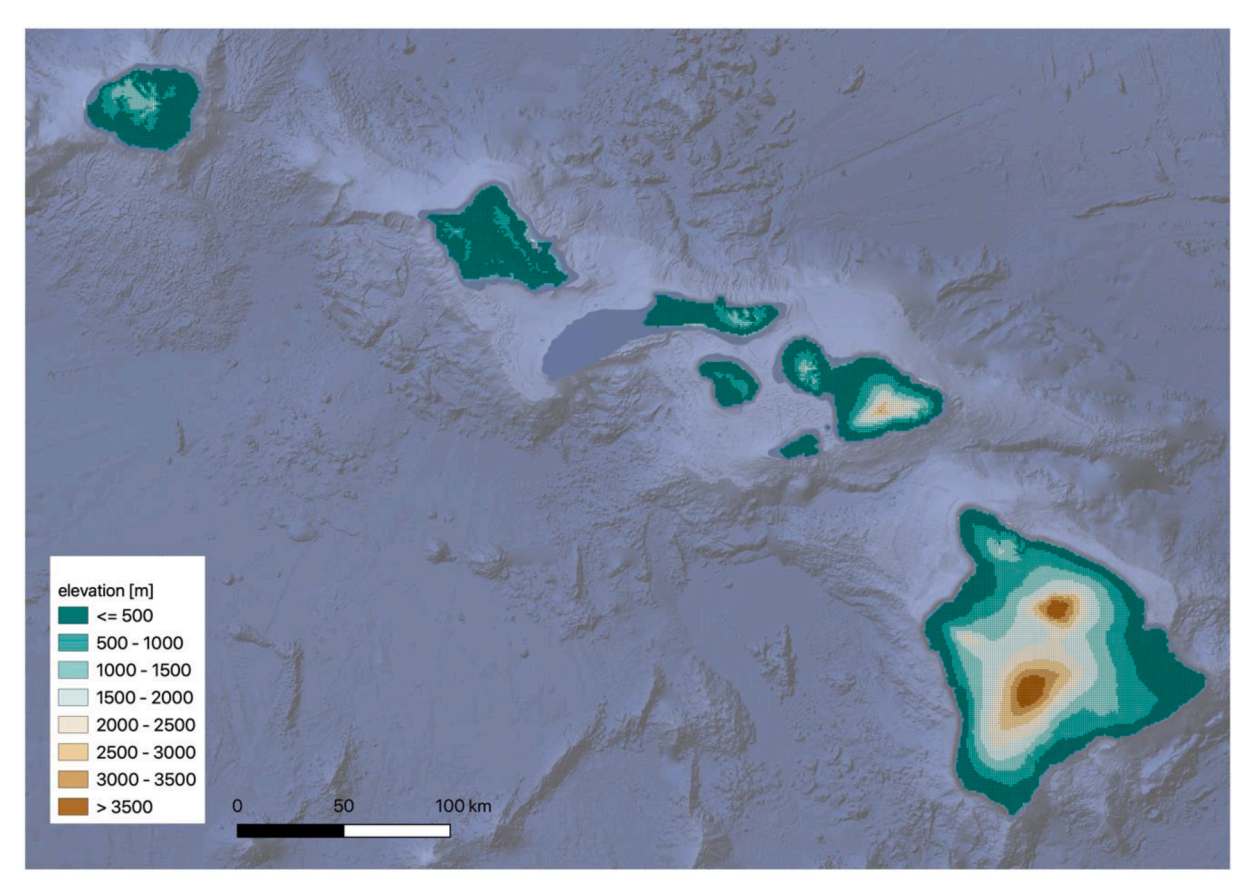


Fig. 3. 1-km VIC model grid over Hawai'i. The model grid boxes (excluding the oceans) are color-coded by elevation.

Table 2 GCM ensemble mean (μ) and standard-deviation (σ) of the VIC model domain-wide late-21st century (2070–2099) changes under RCP4.5 and RCP8.5 relative to the historical period (1970–1999). P: precipitation, ET: Evapotranspiration, RO: Runoff. Domain-wide value is computed with the median of all the grid cells within the domain

		ΔT [°C]		ΔP [mm/yr]		ΔET [mm/yr]		ΔRO [mm/yr]	
		RCP4.5	RCP8.5	RCP4.5	RCP8.5	RCP4.5	RCP8.5	RCP4.5	RCP8.5
Alaska	$\mu \ \sigma$	3.5 1.1	6.2 1.8	130 25	207 44	26 12	43 20	92 19	149 44
Hawai'i	μ σ	1.8 0.6	3.2 0.9	-13 109	41 142	13 25	30 32	-19 86	19 115

Hawai'i

In Hawai'i, we use the daily step, water-balance mode, which is the same model configuration as the CMIP5-based CONUS hydroclimate projection studies (Reclamation 2014, 2020), because there is little soil freeze-thaw process in the islands. Because the spatial variability of precipitation is extremely high (Giambelluca et al. 2013) over the small domain (16,640 km²), we configure the model at a nominal resolution of 1 km (\sim 930 m in longitude and \sim 990 m in latitude or 0.009-degree) for a total of 18,008 grid boxes. The model domain and topography are shown in Fig. 3. Vegetation parameters in Hawai'i including LAI and albedo are taken from the same vegetation library that links land cover types to VIC vegetation related parameters as in the previous CONUS CMIP5 hydroclimate projection work (Reclamation 2014). Land cover data are based on the 500-meter Moderate Resolution Imaging Spectroradiometer (MODIS) derived International Geosphere-Biosphere Programme IGBP classification (MCD12Q1; Friedl and Sulla-Menashe 2019).

Future mean changes

This section presents changes in 30-year mean of temperature and moisture fluxes (precipitation, evapotranspiration and total runoff) for two future periods-mid-21st century (2040-2069) and late-21st century (2070–2099)— relative to the historical period (1970–1999) under RCP8.5. Table 2 summarizes 10 GCM ensemble mean as well as the spread (standard-deviation) of the VIC model domain-wide late 21st century changes in temperature and moisture fluxes for RCP4.5 and RCP8.5. Overall, Alaska exhibits smaller inter-GCM spread for moisture fluxes than Hawai'i where ensemble standard deviation exceeds ensemble mean. Both regions exhibit small uncertainty in temperature change. It should be noted that ensemble mean and spread of moisture fluxes vary spatially within the domains for both states. For example, the increase in runoff is projected over the entire Alaska, except that Southeast Alaska exhibits large runoff decrease due to decreased glacier extent (as discussed in section 3.1). Details of the simulations from individual GCMs (historical mean, mid-21st century and late-21st century changes under RCP4.5 and RCP8.5) are provided in supplemental

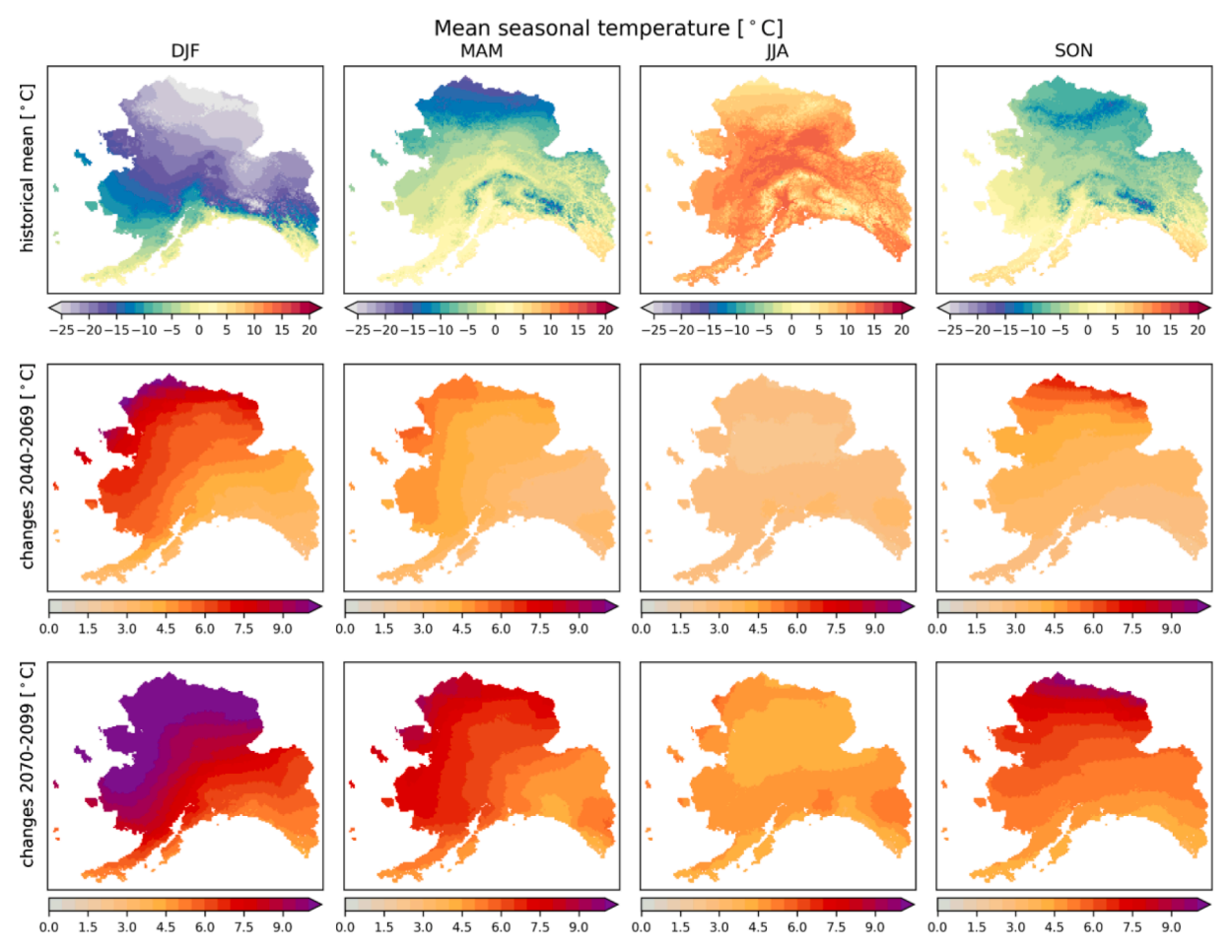


Fig. 4. Alaska ensemble mean seasonal air temperature [°C] during the historical (1970–1999) period (top row) and changes for the mid-century period (2040–2069; 2nd row) and late-century period (2070–2099; 3rd row) under RCP8.5, relative to the 1970–1999 period.

material. The following subsections provide more details on climate change for each region.

Alaska

The ensemble of downscaled GCM annual mean temperature increases by 9 °C along the Arctic Ocean and by 4 °C along the Gulf of Alaska by the end of the 21st century (Table1 and also shown in Fig. S7-AK for individual GCMs). Fig. 4 shows the degree of warming depends on the season, with the strongest warming during the winter season along the Arctic Ocean. The same warming pattern occurs for the RCP4.5 scenario (Fig. S6-AK), but warming is 2–4 °C less than RCP8.5.

Fig. 5 shows annual maximum snow water equivalent (SWE) and ice water equivalent (IWE) during the historical period and their changes for the mid-21st and late-21st century periods for the RCP8.5 scenario. Large reductions in seasonal snowpack (50–100 %) are seen along the Gulf of Alaska and Bering Sea in the future. However, precipitation increases (shown in Fig. 6) contribute to snowpack increases across the interior and North Slope of Alaska. Finally, glaciers still remain in the late 21st century even in the RCP8.5 scenario, but will have much smaller extents due to larger summer time ice melt.

Fig. 6 shows the ensemble mean of annual precipitation, evapotranspiration and total runoff during the historical period and their changes for the mid-21st century and late-21st century periods. Overall, all the moisture fluxes increase progressively during the 21st century. However, the increase in precipitation generally contributes to greater increases in total runoff than evapotranspiration across most of Alaska. In other words, runoff ratio increases by up to 0.1.

For some mountainous areas in southeastern Alaska where glaciers exist at present (Fig. 5), model results show different evapotranspiration and runoff projection compared to the rest of Alaska (Fig. 6). For evapotranspiration, in these areas, weak negative latent heat fluxes (heat transfer from the atmosphere to the glacier surface) or condensation can occur during the summer months, which contribute to additional ice melt. The small increase in condensation (i.e., negative evaporation flux) is projected where glaciers still exist in the future. Large runoff decreases occur in the lower elevations where the glaciers are completely depleted (See Fig. 5), due to the future loss of runoff contributions from glacier ice melt.

Differences between the emissions scenarios (Fig. 7) amount to 200 mm/yr more precipitation for RCP8.5 than RCP4.5. Despite greater increases in precipitation and stronger warming in RCP8.5 than RCP4.5, projected evapotranspiration is much less sensitive than projected runoff to the choice of the emissions scenario. There is a very small area of reduced evapotranspiration for RCP8.5 as compared to RCP4.5 over the mountains in Southeast Alaska where glaciers exist both under RCP8.5 and RCP4.5. In such a case, the higher temperatures under RCP8.5 lead to more negative latent heat fluxes or condensation over glacier fields than RCP4.5. Greater increase in precipitation under RCP8.5 than RCP4.5 explains the difference in the runoff change between two RCPs over Alaska. However, RCP8.5 exhibits larger runoff reductions than RCP4.5 in a small part of the mountainous areas in Southeast Alaska. In low elevations in these areas, the runoff contribution from glaciers is lost in the future when glaciers disappear under RCP8.5, but glaciers may remain and ice melt continues producing large runoff under RCP4.5.

 $\label{fig:prop:section} \textbf{Fig. 8} \ \text{shows the long-term annual cycles of moisture fluxes and state}$

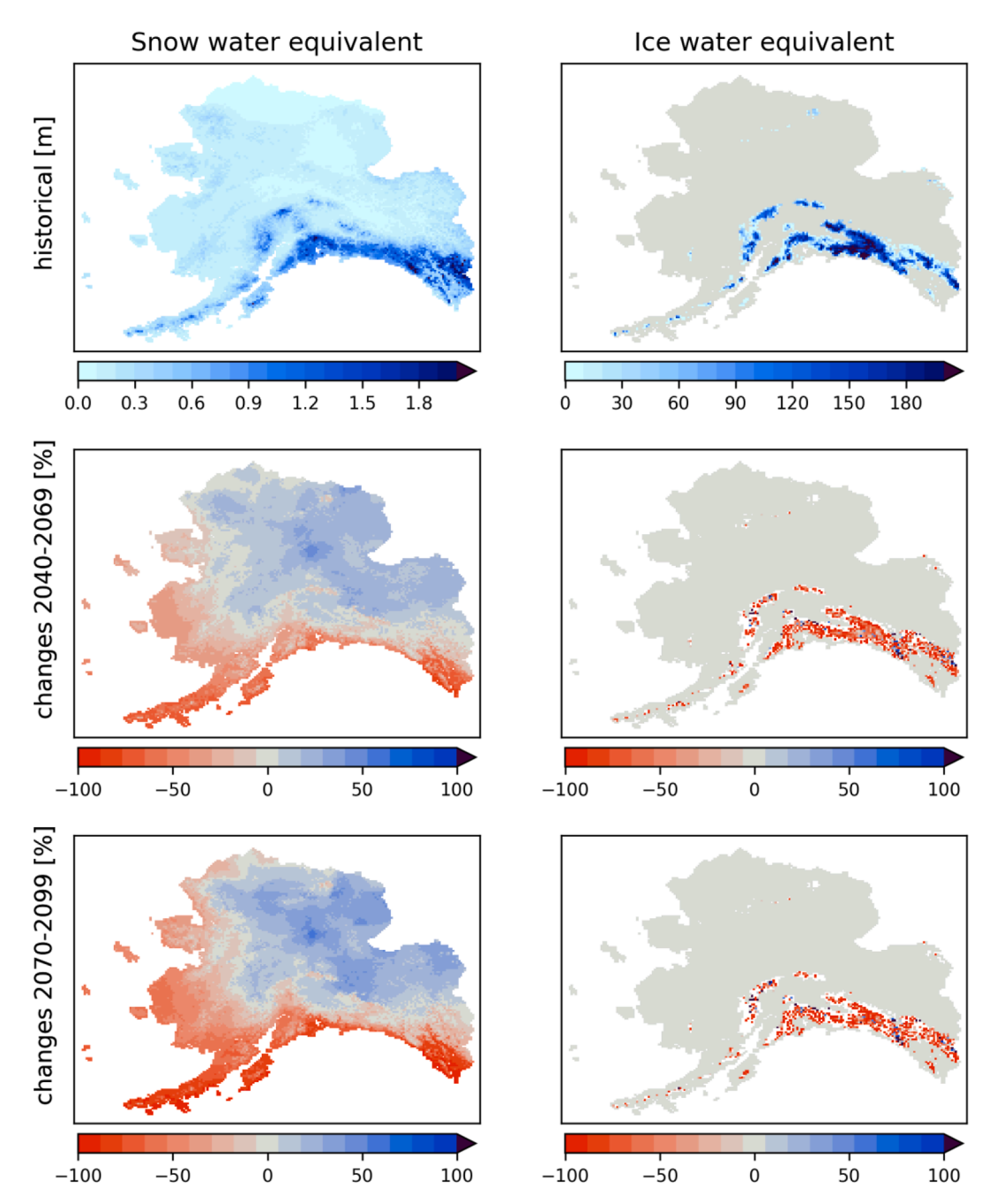


Fig. 5. Alaska ensemble mean annual peak snow water equivalent (left column) and ice water equivalent (right column) during the historical (1970–1999) period (top row) and percentage changes relative to the historical period for the mid-century period (2040–2069: 2nd row) and late-century period (2070–2099: 3rd row) under RCP8.5. White pixels in percent change indicate complete glacier loss.

changes at monthly scale over the three basins shown in Fig. 2: the Copper basin located in Southeast Alaska, where a large portion of runoff is driven by glacier melt; the Teslin basin, which is one of the headwater basins of the Yukon River; and the Colville basin located on the North Slope. All three basins exhibit different historical period precipitation seasonality. While future seasonal patterns remain similar to the historical period, there are differences between individual GCMs. Basin-wide evapotranspiration increases during the summer months with much less inter-model spread than precipitation and runoff. During the winter season, evapotranspiration remains very small because there is little to no downward shortwave radiation regardless of the climate change scenario.

Runoff seasonality and its changes are very different from one basin to another. Two peaks are seen during the historical period in the Colville basin; the first peak due to snowmelt and the second peak driven by summer precipitation. These two peaks also occur in the late-century period with little timing shift (Fig. 8). Hydrologic changes over the Teslin basin are similar to the Colville basin, but with a less pronounced precipitation driven runoff peak during the summer months. For the Teslin basin, snowmelt is projected to begin earlier and increase in rate in the late-century, leading to earlier runoff, and melt-water contributing more to surface runoff than soil moisture recharge resulting in higher peak runoff (Fig. 8). Finally, the Copper basin exhibits an intriguing reduction in total runoff and shift in runoff seasonality because of the large glacier coverage during the historical period and projected future glacial loss. There is a slight shift to more spring runoff due to increased spring snowmelt, and a drastic reduction in summer runoff due to the loss of glacier coverage and summer ice melt runoff

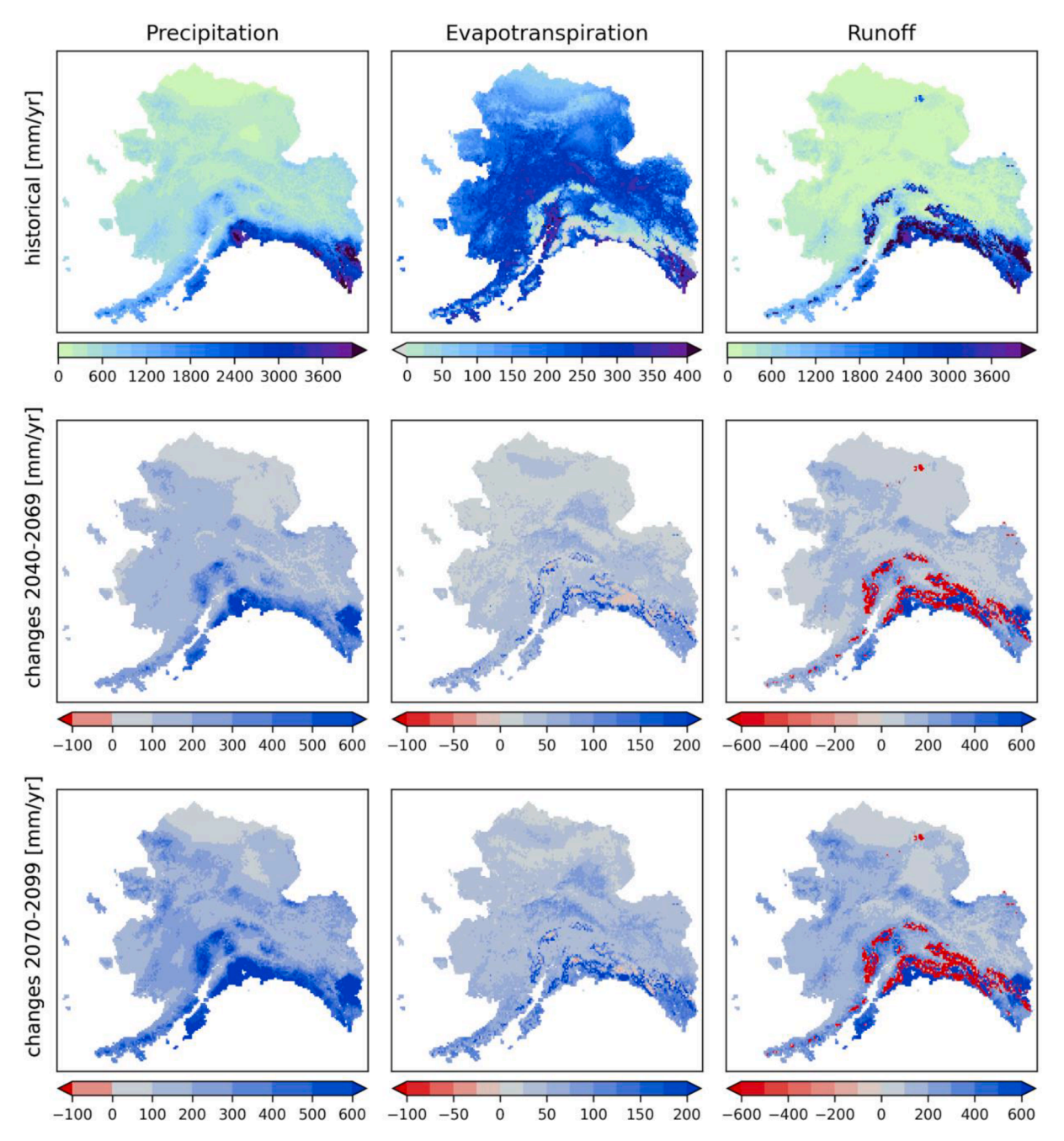


Fig. 6. Alaska ensemble mean annual fluxes during the historical (1970–1999) period (top row) and changes for the mid-century period (2040–2069, 2nd row) and late-century period (2070–2099, 3rd row) under RCP8.5 relative to 1970–1999 period.

contributions (Fig. 8).

Hawai'i

Temperature increases by the late 21st century are 2 °C for RCP4.5 and 3 °C for RCP8.5 over Hawai'i (See Table 2) with little spatial variability. Variability in the temperature increases among the 10 GCMs is relatively small compared to Alaska, with Coefficient of Variations of 0.2 and 0.3 over the domain for RCP4.5 and RCP8.5 respectively. Additionally, there is little seasonality in the temperature increase (not shown). Unlike temperature, uncertainty in precipitation change for the late 21st century across the GCMs is large as shown in Fig. 9 (also illustrated with the native GCMs in Fig. 1). Fig. 9 also shows the future change in total runoff is closely linked to that in precipitation, indicating that the uncertainty in hydrologic projections comes largely from the

driving GCM's precipitation. However, evapotranspiration is likely to increase even with precipitation decreases in the future (except that GCMs producing large precipitation reduction such as MIROC5 may reduce evapotranspiration).

Fig. 10 shows spatial patterns of the ensemble mean change in moisture fluxes for the mid- and late-21st century periods relative to the historical period. Focusing on the ensemble mean change, overall Hawai'i receives increased precipitation by the late 21st century, leading to increased total runoff. This increase is the largest on the windward (east) side of the islands. However, the ensemble mean precipitation decreases across nearly all portions of the islands in the mid-21st century, indicating the trend in climate change may not be a monotonic increase.

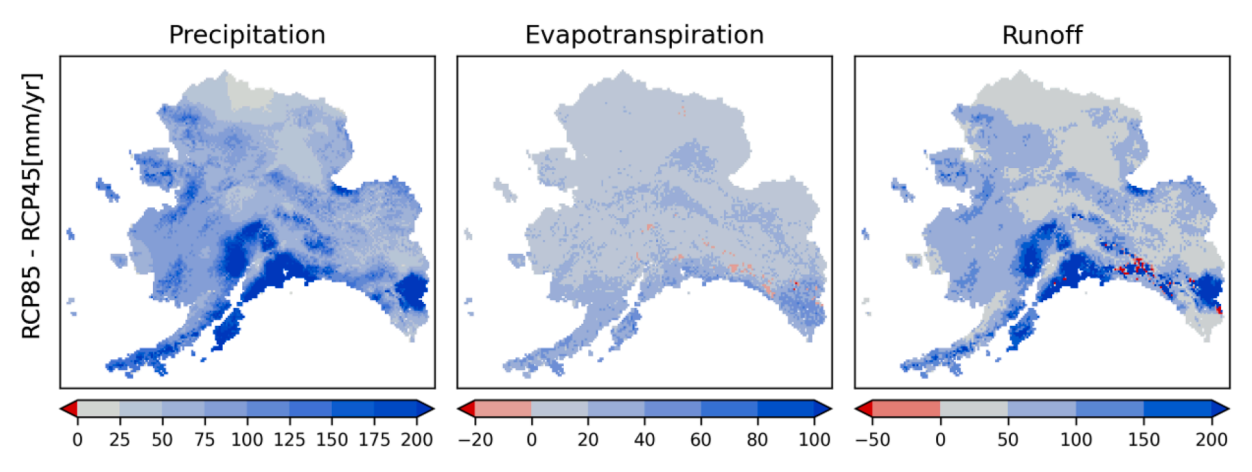


Fig. 7. Comparison of changes in all the Alaska fluxes for the late-century period (2070–2099) between the two RCPs (RCP8.5 minus RCP4.5). GCM ensemble mean values are used.

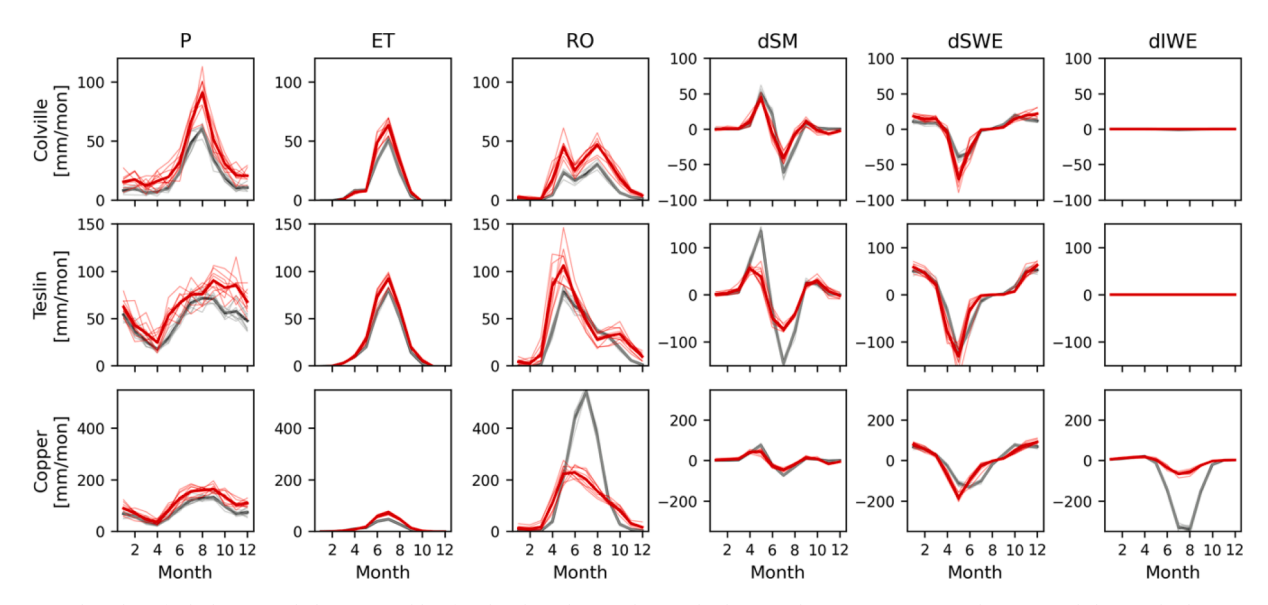


Fig. 8. Seasonal cycles of Alaska water balance variables for the three basins during the historical (1970–1999) period (gray) and during the late-21st century (2070–2099) period (red) under RCP-8.5. Thin lines denote individual GCMs and a thick line denotes the mean of all the GCMs. State variables (dSM: soil moisture, dSWE: snow water equivalent, dIWE: ice water equivalent) are monthly changes.

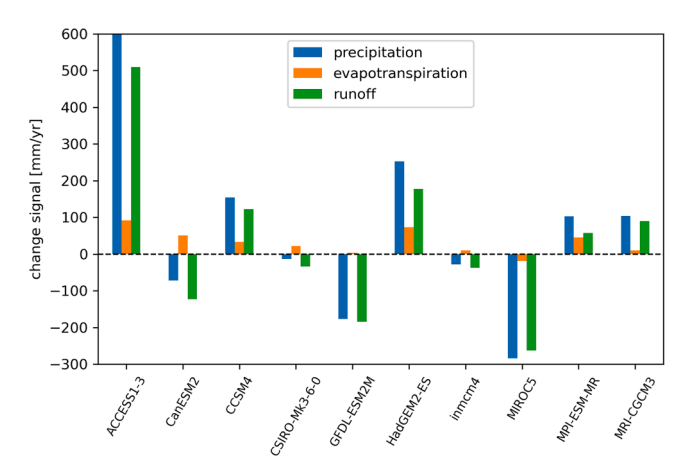


Fig. 9. Hawai'i domain average moisture flux changes for the late 21st century (2070–2099) for each GCM under RCP8.5.

Discussion

The hydrologic modeling presented in this paper is a step forward for climate impact assessments needing hydrologic projection information across Alaska and Hawai'i. However, there are many aspects of these projections that would benefit from additional attention and serve as motivation for future research.

Relationships to previous work

Our projected seasonal warming pattern in Alaska (Fig. 4) is consistent with the results from Walsh et al. (2018), who downscaled five CMIP5 GCMs using the monthly delta method (see Walsh et al. 2018 for method descriptions), which is a simpler downscaling technique than BCSD. In colder regions e.g., high-elevations, interior, the North Slope, projected increases in precipitation (Fig. 6) result in projected increases in snowfall and snow water equivalent (Fig. 5) because the air temperature likely remains sub-freezing in winter even with extensive future warming. This agrees with previous work (Littell et al. 2018, Lader et al. 2020; Newman et al., 2020). However, warming in spring, despite of less degree than winter, can impact snowmelt process as present spring

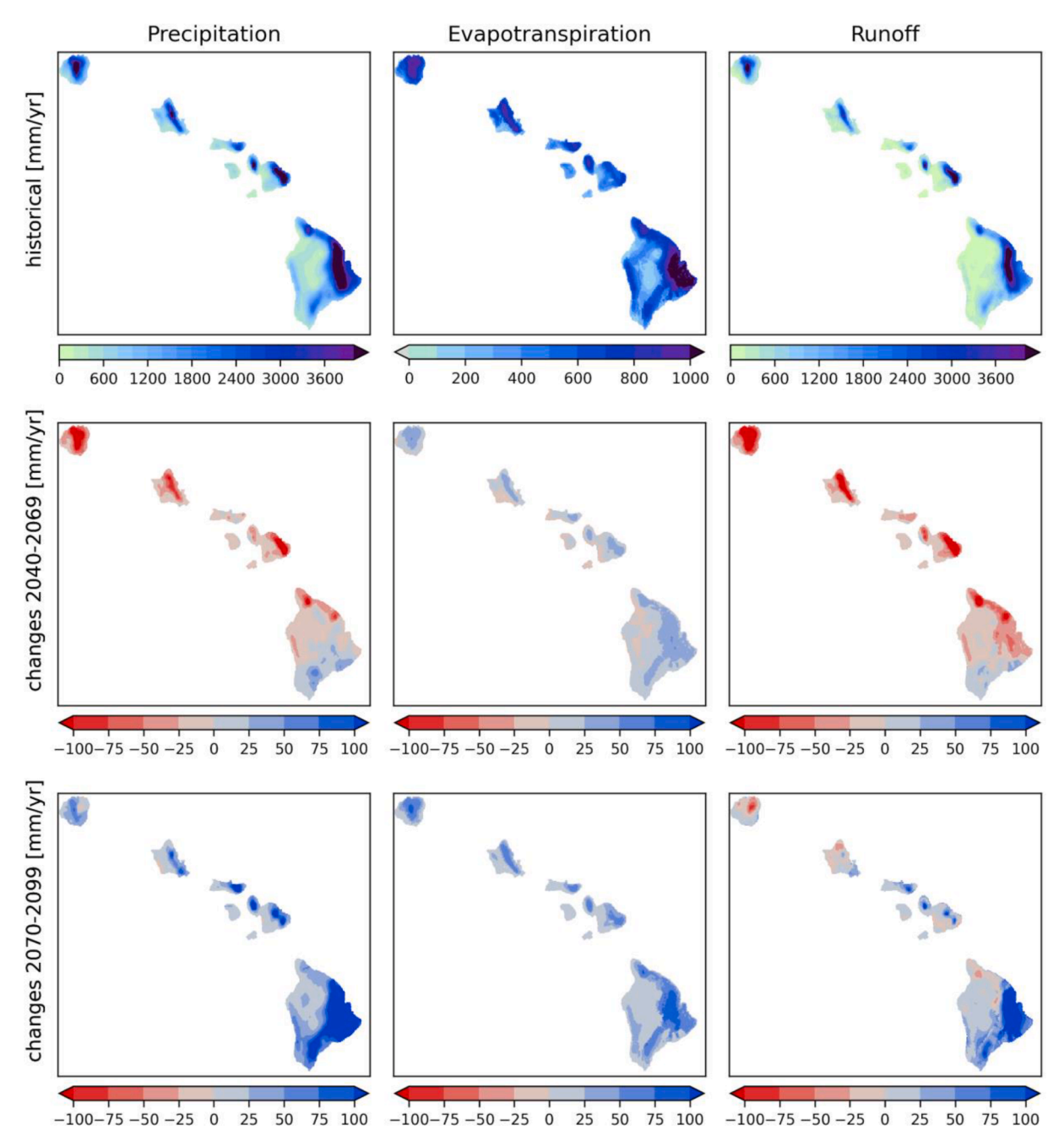


Fig. 10. Hawai'i ensemble mean annual fluxes during the historical (1970–1999) period (top row) and changes for the mid-century period (2040–2069, 2nd row) and late-century period (2070–2099, 3rd row) under RCP8.5 relative to 1970–1999 period.

temperature is closer to 0 °C, resulting in earlier snowmelt runoff onset (Fig. 8). Additionally, our historical simulations show weak negative latent heat flux for some glaciated regions in southeastern Alaska (Fig. 6) during summer. This agrees with observations over humid, high latitude glaciers where incoming shortwave radiation is limited (Sicart et al. 2008). During the future periods, the glaciers remain in some areas in southeastern Alaska (Fig. 5). These areas may see an increase in condensation because the warmer and wetter atmosphere contains the larger amount of moisture in near-saturated condition, causing greater moisture gradient between the glacier surface and atmosphere. This enhances ice-melt during summer.

Across Hawai'i, Frazier and Giambelluca (2017) have shown an overall drying trend based on their precipitation trend analysis spanning 1920–2012. Our projections indicate general statewide drying through mid-century (Fig. 10) and a more neutral (Fig. S8-HI) or wetter at the

end of century (Fig. S9-HI) depending on RCP. Some other statistical and dynamical downscaling efforts over Hawaii show a more pronounced dipole of more precipitation on windward and less precipitation on leeward slopes for the 2070–2099 period using RCP8.5 (Elison Timm et al. 2015; Zhang et al. 2016) which differs from our results, while other dynamic downscaling results are more similar to the BCSD results presented here (Xue et al. 2020). The attribution of these differences is an open research question and could be due to several factors. Some of the spread across different projections (and models) in Hawai'i could be due to differences in the representation of changes in the expansion of the Hadley circulation in the subtropical Pacific and how statistical and dynamical downscaling methodologies represent those changes. Additionally, the BCSD scheme directly downscales precipitation which may limit the spatial flexibility of method to represent complex change patterns within one GCM grid cell such as one of the Hawaiian Islands,

while the work of Elison Timm et al. (2015) uses additional circulation variables (e.g. 700 hPa moisture advection) which may induce different future spatial patterns. Furthermore, temporal patterns in the 20th century streamflow in Hawai'i are correlated with the precipitation patterns and ENSO and PDO phases (Bassiouni and Oki 2013). Thus, uncertainty in hydroclimate projections across Hawai'i seen in Fig. 9 are likely to be affected by how each GCM captures such large-scale dynamics. For example, it is likely some GCMs exhibit positive PDO phase while others are in the negative phase in the same period in the future.

Sources of uncertainty

Our hydrologic projections incorporate uncertainty due to the choice of the GCM and emission scenarios. Although many studies have indicated that those two components of the modeling chains are the primary sources of uncertainty for the evaluation of hydrologic impacts, particularly the long-term runoff volume (e.g., Kay et al. 2009; Prudhomme and Davies 2009; Najafi et al. 2011; Bennett et al. 2012; Chegwidden et al., 2019; Surfleet and Tullos 2013; Addor et al., 2014; Vano et al. 2014), other components—downscaling methods and hydrologic modeling—can contribute to substantial uncertainty in the hydroclimate projections and should not be neglected (Clark et al., 2016).

The source of uncertainty in climate downscaling includes not only the choice of SD method (Gutmann et al., 2014; Mizukami et al. 2016), but also input training data uncertainty across both domains (Newman et al. 2019; Newman et al., 2020) which can also lead to different future projections of hydrologically relevant variables (Wootten et al., 2021). Two notable impacts are that different SD methods can produce different wet-day frequency (the number of days with precipitation; Gutmann et al., 2014) which, with associated cloud frequency differences, affects estimates of shortwave radiation (Mizukami et al. 2016), and different training data can impact the representation of change of daily maximum precipitation.

The implication for this work is that there may be an underestimation of the spread of possible future meteorological (e.g., precipitation and temperature) and hydrological (e.g., evapotranspiration, runoff) change, particularly in regions of poorly observed complex topography or in areas of transition from historical snow to snow-free futures (e.g., Southeast Alaska). In these areas the training data will have the largest impact on projected meteorological and hydrological change because of large uncertainty in local-scale climate representation such as lapse rates, cold-pool and so on. Furthermore, in such areas, SD methods that account for topographic effects on local scale climate may be advantageous (Fiddes and Gruber 2014).

Work on dynamically downscaled climate simulations has been undertaken for Alaska (Lader et al. 2017; Newman et al., 2020) and Hawai'i (Zhang et al. 2016; Xue et al., 2020). Future projected changes in Zhang et al. (2016), Xue et al. (2020) and Newman et al. (2020) are from dynamically downscaled simulations based on the pseudo-global warming (PGW) approach (e.g., Schär et al. 1996, Rasmussen et al. 2011), in which a regional climate model was run at high-resolutions (4 km for Alaska, 1.5 km for Hawai'i) with historical atmospheric boundary conditions and perturbed boundary conditions based on an end-ofcentury (2071-2099) ensemble mean of CMIP5 GCMs for RCP8.5. For Alaska, both the PGW-based climate projection and the individually downscaled GCMs of Lader et al. (2017) show a similar magnitude and spatial pattern of precipitation change to our ensemble mean of BCSD downscaled precipitation change under RCP8.5 (Fig. 5 in Newman et al., 2020). For Hawai'i, Xue et al., (2020) shows positive statewide precipitation changes, though an increase in precipitation is seen in the windward side of the islands mainly during the wet season (November through April). Zhang et al. (2016) shows a pronounced dipole of future dryer leeward and wetter windward slopes for both dry and wet seasons. Differences between the PGW simulations and the BCSD dataset described here could be attributed to circulation differences in the future climates as well as the methodological differences (e.g., GCM choice,

spatial resolution, bias-correction and so on) across statistical and dynamical downscaling methods.

For hydrologic modeling, the VIC model parameters used here are essentially uncalibrated (Section 2). Mendoza et al. (2015) illustrated that hydrologic model calibration reduces uncertainty in climate sensitivity to simulated hydrologic responses arising from hydrologic model choices. Though hydrologic model calibration is common in previous basin-scale hydrologic projection studies (e.g., Bennett et al., 2012), large domain studies pose a significant challenge in estimating spatially distributed hydrologic model parameters and is an area of active research (Oubeidillah et al. 2014; Mizukami et al. 2017; Rakovec et al., 2019; Yang et al. 2019). Other recent studies (Vidal et al. 2016; Chegwidden et al. 2019) have shown that hydrologic model choices can contribute to greater uncertainty relative to the other modeling chain components, particularly for low flow. Baseflow production, which dominates runoff for low flow periods, particularly in dry environments, is largely determined by soil process representation in a hydrologic model. In addition, the complexity of evapotranspiration formulations implemented in hydrologic models varies depending on the parameterization (e.g., PET formulation) and land cover representations. This affects runoff, particularly during the warm season (Vidal et al., 2016). Therefore, modeling that uses multiple hydrologic models with multiple parameter sets would better represent uncertainty due to hydrologic

There are several implications of the use of a single uncalibrated model for the hydrologic model results presented here. First, the spread or uncertainty of our hydrologic projections will be underestimated because of the use of one model. Second, the reliability of the climate sensitivity of the hydrologic model, or the model representation of hydrology under different climates is unknown. Third, use of the hydrologic projections in other impact models (e.g., stream routing and temperature models) would likely require additional, carefully crafted bias correction of predicted hydrological variables such as snow water equivalent, evapotranspiration, and runoff.

The land cover data used for this study are temporally static throughout the 150-year simulation periods, though future vegetation cover is likely to differ from the present time due to climate change (and related disturbances such as fire) as well as human interventions (agricultural practices, afforestation and deforestation). The future land cover scenario dataset such as the Land-Use Harmonization project dataset (Hurtt et al. 2020) based on RCPs may be a useful dataset to examine the impacts on hydrologic response based on both climate and land cover scenarios.

Hydrologic modeling process challenges in Alaska and Hawai'i

For mountainous parts of Southeast Alaska, glaciers as well as seasonal snow cover affect moisture fluxes i.e., runoff and evapotranspiration. The glacier retreat in Southeast Alaska is likely to accelerate in the future based on current trend (Bevington and Menounos 2022), likely impacting future water availability. Beamer et al. (2016) suggested that snow and ice melt contribute as much as 80 % of the total runoff over the glacierized areas in the drainage basins along the Gulf of Alaska. For modeling runoff production from glaciers, the initialization of glacier ice volumes is critical. This is because our results indicate that ice melt contributes a large portion of total runoff during the present time and initial ice volumes affect the timing of large or even complete glacial retreat in the future. Additionally, our results on the reduction of summer glacier runoff in the future are qualitatively similar to those of Beamer et al. (2017). However, they showed that future runoff change is significantly influenced by estimated future glacier extent, or ice volume. Furthermore, for basins where glaciers exist at present such as Southeast Alaska, errors in glacier initialization affect the simulations for a much longer time period compared to other states such as soil moisture because glacier dynamics are transient throughout our simulation period (150 years). Thus, improving glacier initialization and

Practical implications

Environmental and resource assessments conducted by many municipal, tribal and federal entities (e.g., US federal agencies such as the US Fish and Wildlife Service Species Status Assessments or Water Resource Inventory Assessments, the US Forest Service Forest Plans and vulnerability assessments, US National Park Service Resource Stewardship Strategies, and tribal adaptation plans) now seek to include climate impacts on resources of concern. Changes in terrestrial and aquatic habitats, species' abundance and distribution, disturbances (such as fires and insects), and hydrologic changes are often considered in vulnerability assessment and adaptation planning at sub-regional to local scales. Methodologically consistent sets of climate and hydrology projections help these agencies to plan for climate impacts in the water resources sector as well as other hydrologically driven resources. Moreover, as planning and adaptation practices converge toward risk-based scenario planning, considering a wider range of plausible outcomes is desirable. The scenarios should address major sources of climate uncertainty such as climate model differences, emission trajectories, and downscaling methods (Snover et al. 2013; Clark et al., 2016; Vano et al., 2014; Terando et al., 2020)

In the absence of resource-specific information, potential climate impacts on resources of concern are often assessed using whatever projections are available (e.g., Hayward et al., 2017). Resource managers in Alaska and Hawai'i have general resource-planning information needs similar to those of their counterparts in the CONUS states, but work in climatic, hydrologic, and ecological contexts with no close CONUS analogs. In Alaska where rates of temperature change are over twice the global average, and Hawai'i, where unique climates and ecosystems prevail, practitioners to date have been faced with a paucity of projections, and methods for assessing and using them, compared to the information available for the CONUS.

Ideally, climate information is tailored to the decision contexts within which managers work (Enquist et al., 2017) to distinguish and evaluate the climate change impacts that may be reduced through adaptation (e.g., Thompson et al., 2021). Moreover, potential climate change adaptation decisions can have a stronger scientific foundation if they are supported by hydrologically-relevant scenarios consisting of climate models, downscaling, and hydrologic modeling tailored to the region of interest. The downscaled hydroclimate projections presented in this paper provide such a foundation over larger domains and for more scenarios than were previously available for Alaska and Hawai'i These scenarios can provide a path towards adaptation planning that uses a framework like Resist, Accept, Direct (RAD; Schuurman et al., 2020; Thompson et al., 2021). The decision whether to Resist (act to maintain desired conditions despite climate trajectories), Accept impacts of climate change without significant intervention, or actively Direct those changes with different management practices may depend on projections that address specific impact pathways, a carefully constructed approach to uncertainty, or both.

In Alaska, water resources planning for communities in Southeast Alaska offers an example of the need for hydrologic projections. Historically these communities have relied on small-scale projects for municipal water resources and hydropower generation. A 2018–2019 drought in this region known for its rainforests challenged many of these projects' abilities to provide reliable water and/or power (Bathke et al., 2019), and the implications of future climate changes remain poorly understood. For these projects, the hydrologic impacts of climate change, such as watershed-scale transitions from snow to rain dominance and year-round runoff changes, are much more important than the magnitude change in seasonal temperature or precipitation, and these hydrologic impacts might not be readily inferable without process-based hydrologic modeling. These planning efforts also frequently require approaches that address major sources of uncertainty such as climate variability and model uncertainty. Cherry et al. (2010) noted that even planning for historical variability in these systems was challenging due to limited data availability.

In Hawai'i, available downscaled climate projections are also relatively few in number and, prior to the results presented here, no statewide process-based hydrological estimates for downscaled future climate have been made. The new hydroclimatic projections for Hawai'i represent a significant milestone, providing estimates of changes in key variables affecting water resources, agriculture, terrestrial and aquatic ecosystems, drought, flood, and wildfire hazard, and other sectors. The finding of wide variability in future precipitation change projections derived from different GCMs and associated high uncertainty in projected changes in hydrological processes underscores the need to make resilient decisions in resource management, e.g., for sustaining potable water supply, and natural hazards, e.g., flooding, adaptation planning in Hawai'i.

modeling may be one of the highest priorities for future hydrologic projection work in the glacier basins.

A second challenge in Alaska is the lack of detailed mapping of soil properties and deep (>2m) permafrost to simulate changes in baseflow and infiltration below the active layer as permafrost thaws. Our VIC model uses three soil layers with a total depth of 3 m to simulate soil thermal and moisture fluxes. The presence or absence of deep continuous permafrost or yedoma (ice-rich soils) below the simulated active layer could control both energy and water balance through controls on both infiltration and preferential flow paths (e.g., Jin et al. 2022) but are poorly mapped over vast portions of Alaska.

In Hawai'i, groundwater is the primary water resource for drinking water and agricultural use. Mair (2019) estimated groundwater recharge that does not reemerge at surface accounts for approximately 10–60 % of precipitation in Island of Maui, while runoff accounts for 10–40 % of precipitation. Hence, a substantial portion of the Hawai'i water balance is not captured in a conventional watershed mass balance. This deep groundwater discharges via submarine pathways to the ocean, besides withdrawals for municipal and agricultural water use. Our modeled water balance excludes this ground water recharge (i.e., precipitation input is partitioned into runoff, evapotranspiration and storage in soil). The estimated long-term water balance (Fig. 10) is closed

water balance among precipitation, evapotranspiration and runoff. Therefore, it is important to note that runoff estimated in this paper would be more accurately termed surplus, i.e., the sum of runoff and groundwater recharge. Although modeling groundwater flow in Hawai'i is complicated due to the existence of volcanic rock with various permeability and impermeable dikes, which impede lateral groundwater, it is desirable to include the vertical percolation process at the model bottom layer to estimate groundwater recharge.

Another challenge in hydrologic modeling in Hawai'i may be capturing highly heterogeneous spatial patterns in evapotranspiration. The spatial pattern of evapotranspiration during the historical period in Fig. 10 is different from Giambelluca et al., (2014), who used the Penman and Monteith (Monteith 1973) method with 250-meter resolution meteorological data as well as detailed land cover and agriculture information. Our estimated evapotranspiration spatial pattern resembles that of precipitation during the historical period (i.e., highest ET area corresponds to the wettest area in the islands) while Giambelluca et al., (2014) shows that the highest ET occurs in the highly irrigated, dry areas where both moisture and solar radiation is abundant. Capturing a more accurate evapotranspiration pattern at high resolution modeling needs detailed spatial information on agriculture and corresponding irrigation practice.

Conclusions

We have generated 21st century downscaled climate and hydrology projection datasets over Alaska and Hawai'i. The projections are based on 150-year continuous hydrologic model simulations forced by 10 downscaled GCMs from the CMIP5 archive for both the RCP 4.5 and RCP 8.5 scenarios. Prior to this work, there were only limited hydroclimate focused projection studies and datasets available for both regions that included state-wide estimates of the surface water balance. The products will provide information on the first-order climate and hydrologic projections and their uncertainties during the rest of the 21st century suited in many cases for water-resource adaptation planning. Our results indicate increases in precipitation, evapotranspiration, and runoff over Alaska, but glacier retreat greatly reduces runoff over currently glaciated areas. In contrast to Alaska, for Hawai'i, large uncertainties in future moisture fluxes dominate the model results, especially runoff, which are driven by large uncertainty in precipitation change.

There are needs for future improvements in both Alaska and Hawai'i, due to specific hydroclimate processes that are unique to each region, including transient glacier hydrology in Alaska and subsurface percolation to ocean connected aquifers in Hawai'i. There are significant local meteorological processes in need of further refinement as well. In Hawai'i, future changes in the trade-wind inversion (Xue et al., 2020) and its effect on orographic precipitation are not represented currently, and in Alaska, the high coastal orography combined with the role of sea ice on moisture source regions are missing in the regional climate assessment here.

Data and code availability

Daily and monthly downscaled GCM and VIC outputs, stored in yearly netCDF-4, are archived at https://doi.org/10.5065/c3kn-2y77. The total size of the daily downscaled GCM is 133 GB for Alaska and 151 GB for Hawai'i, while daily VIC outputs are 723 GB for Alaska and 348 GB for Hawai'i. The downscaled GCM dataset includes daily minimum and maximum temperatures and precipitation. The VIC outputs are split into water flux dataset including surface runoff, baseflow, total evapotranspiration, snowmelt and ice melt (only for Alaska) and state dataset including soil moisture, snow water equivalent, and ice water equivalent (only for Alaska). For Alaska, energy fluxes (shortwave and longwave radiation, latent and sensible heat fluxes, and ground heat as well as soil temperature) are also archived. VIC soil and vegetation parameters in NetCDF format are also provided. Finally, the model codes used in this paper are open-source softwares. The VIC source code used in this paper is available at https://github.com/UW-Hydro/VIC/tree/VIC.4.2.glacier .01 and BCSD code is available at https://github.com/pangeo-data/sciki t-downscale/tree/ak-hi-round2.

CRediT authorship contribution statement

Naoki Mizukami: Methodology, Software, Investigation, Formal analysis, Visualization, Writing – original draft, Writing – review & editing, Data curation. Andrew J. Newman: Methodology, Software, Investigation, Formal analysis, Visualization, Data curation, Writing – original draft, Writing – review & editing, Project administration, Supervision. Jeremy S. Littell: Writing – original draft, Writing – review & editing. Thomas W. Giambelluca: Writing – original draft, Writing – review & editing. Andrew W. Wood: Software, Methodology, Writing – review & editing. Ethan D. Gutmann: Software, Writing – review & editing. Diana R. Gergel: Software, Writing – review & editing. Bart Nijssen: Software, Writing – review & editing. Martyn P. Clark: Conceptualization, Writing – review & editing, Funding acquisition, Supervision. Jeffrey R. Arnold: Writing – review & editing, Funding acquisition.

Declaration of Competing Interest

The authors declare that they have no known competing financial interests or personal relationships that could have appeared to influence the work reported in this paper.

Acknowledgements

This work was financially supported by the U.S Army Corps of Engineers Climate Preparedness and Resilience program, and by the National Center for Atmospheric Research (NCAR), which is a major facility sponsored by the National Science Foundation under Cooperative Agreement No. 1852977. The simulations and visualization presented for this paper were produced through the Cheyenne and Casper computational resources (doi:10.5065/D6RX99HX) at the NCAR-Wyoming Supercomputing Center supported by the National Science Foundation and operated by NCAR's Computational and Information Systems Laboratory. We thank Ryan Toohey and three anonymous reviewers for comments that improved the manuscript.

Appendix A. Supplementary data

Supplementary data to this article can be found online at https://doi.org/10.1016/j.cliser.2022.100312.

References

- Abatzoglou, J.T., Dobrowski, S.Z., Parks, S.A., Hegewisch, K.C., 2018. TerraClimate, a high-resolution global dataset of monthly climate and climatic water balance from 1958–2015. Sci. Data 5, 170191. https://doi.org/10.1038/sdata.2017.191.
- Addor, N., Rössler, O., Köplin, N., Huss, M., Weingartner, R., Seibert, J., 2014. Robust changes and sources of uncertainty in the projected hydrological regimes of Swiss catchments. Water Resour. Res. 50, 7541–7562. https://doi.org/10.1002/2014wr015549.
- Addor, N., Newman, A.J., Mizukami, N., Clark, M.P., 2017. The CAMELS data set: catchment attributes and meteorology for large-sample studiesdoi:10.5065/ D6G73C3Q.
- Bahr, D.B., 1997. Global distributions of glacier properties: A stochastic scaling paradigm. Water Resour. Res. 33, 1669–1679. https://doi.org/10.1029/ 97WP00824
- Bassiouni, M., Oki, D.S., 2013. Trends and shifts in streamflow in Hawai'i, 1913-2008: TRENDS AND SHIFTS IN STREAMFLOW IN HAWAI'I. Hydrol. Process. 27 (10), 1484-1500.
- Bathke, D.J., Prendeville, H.R., Jacobs, A., Heim, R., Thoman, R., Fuchs, B., 2019. Defining drought in a temperate rainforest. Bull. Am. Meteorol. Soc. 100 (12), 2665–2668. https://doi.org/10.1175/BAMS-D-19-0223.1.
- Baumberger, C., Knutti, R., Hirsch Hadorn, G., 2017. Building confidence in climate model projections: an analysis of inferences from fit. Wiley Interdiscipl. Rev. Clim. Change 8 (3), e454.
- Beamer, J.P., Hill, D.F., Arendt, A., Liston, G.E., 2016. High-resolution modeling of coastal freshwater discharge and glacier mass balance in the Gulf of Alaska watershed. Water Resour. Res. 52 (5), 3888–3909.
- Beamer, J.P., Hill, D.F., McGrath, D., Arendt, A., Kienholz, C., 2017. Hydrologic impacts of changes in climate and glacier extent in the Gulf of Alaska watershed. Water Resour. Res. 53 (9), 7502–7520.
- Bennett, K.E., Werner, A.T., Schnorbus, M., 2012. Uncertainties in hydrologic and climate change impact analyses in headwater basins of british columbia. J. Clim. 25, 5711–5730. https://doi.org/10.1175/jcli-d-11-00417.1.
- Bevington, A. R., and B. Menounos, 2022: Accelerated change in the glaciated environments of western Canada revealed through trend analysis of optical satellite imagery. *Remote Sens. Environ.*, 270, 112862, https://doi.org/https://doi.org/ 10.1016/j.rse.2021.112862.
- Chegwidden, O.S., Nijssen, B., Rupp, D.E., Arnold, J.R., Clark, M.P., Hamman, J.J., Kao, S.-C., Mao, Y., Mizukami, N., Mote, P., Pan, M., Pytlak, E., Xiao, M., 2019. How do modeling decisions affect the spread among hydrologic climate change projections? Exploring a large ensemble of simulations across a diversity of hydroclimates. Earth's Future, 010.1029/2018EF001047.
- Cherkauer, K.A., Lettenmaier, D.P., 1999. Hydrologic effects of frozen soils in the upper Mississippi River basin. J. Geophys. Res. Atmos. 104, 19599–19610. https://doi.org/ 10.1029/1999JD900337.
- Clark, M.P., Wilby, R.L., Gutmann, E.D., Vano, J.A., Gangopadhyay, S., Wood, A.W., Fowler, H.J., Prudhomme, C., Arnold, J.R., Brekke, L.D., 2016. Characterizing uncertainty of the hydrologic impacts of climate change. Curr. Clim. Chang. Rep. 2, 55–64. https://doi.org/10.1007/s40641-016-0034-x.
- Elison Timm, O., Giambelluca, T.W., Diaz, H.F., 2015. Statistical downscaling of rainfall changes in Hawaiʻi based on the CMIP5 global model projections. J. Geophys. Res. Atmos. 120, 92–112. https://doi.org/10.1002/2014JD022059.

- Enquist, Carolyn, et al., 2017. Foundations of translational ecology. Front. Ecol. Environ. 15 (10), 541–550. https://doi.org/10.1002/fee.1733.
- Fiddes, J., Gruber, S., 2014. TopoSCALE vol 1.0: downscaling gridded climate data in complex terrain. Geosci. Model Dev. 7, 387–405. https://doi.org/10.5194/gmd-7-387-2014
- Frazier, A.G., Giambelluca, T.W., 2017. Spatial trend analysis of Hawaiian rainfall from 1920 to 2012. Int. J. Climatol. 37 (5), 2522–2531.
- Friedl, M., Sulla-Menashe, D., 2019. MCD12Q1 MODIS/Terra+Aqua Land Cover Type Yearly L3 Global 500m SIN Grid V006. NASA EOSDIS Land Processes DAAC. Last Accessed 2021-09-27 from https://doi.org/10.5067/MODIS/MCD12Q1.006.
- Gergel, D.R., 2019. Modeling the changing roles of snow and permafrost in midhigh-latitude climate systems. University of Washington, PhD Diss.
- Giambelluca, T.W., Chen, Q., Frazier, A.G., Price, J.P., Chen, Y.-L., Chu, P.-S., Eischeid, J. K., Delparte, D.M., 2013. Online Rainfall Atlas of Hawai'i. Bull. Am. Meteorol. Soc. 94, 313–316. https://doi.org/10.1175/BAMS-D-11-00228.1.
- Giambelluca, T.W., X. Shuai, M.L. Barnes, R.J. Alliss, R.J. Longman, T. Miura, Q. Chen, A. G. Frazier, R.G. Mudd, L. Cuo, and A.D. Businger. 2014. Evapotranspiration of Hawai'i. Final report submitted to the U.S. Army Corps of Engineers—Honolulu District, and the Commission on Water Resource Management, State of Hawai'i.
- Gutmann, E., Pruitt, T., Clark, M.P., Brekke, L., Arnold, J.R., Raff, D.A., Rasmussen, R.M., 2014. An intercomparison of statistical downscaling methods used for water resource assessments in the United States. Water Resour. Res. 50, 7167–7186. https://doi.org/10.1002/2014wr015559.
- Hamman, J., and Nijssen, B, 2015: VIC 4.2.glacier. Retrieved from https://github.com/ UW-Hydro/VIC/tree/support/VIC.4.2.glacier.
- Hawkins, Ed, Sutton, Rowan, 2009. The potential to narrow uncertainty in regional climate predictions. Bull. Am. Meteorol. Soc. 90 (8), 1095–1108. https://doi.org/ 10.1175/2009BAMS2607.1.
- Hay, L.E., McCabe, G.J., 2010. Hydrologic effects of climate change in the Yukon River Basin. Clim. Change 100, 509–523. https://doi.org/10.1007/s10584-010-9805-x.
- Hayward, G.H., Colt, S., McTeague, M.L., Hollingsworth, T.N., 2017. Climate change vulnerability assessment for the Chugach National Forest and the Kenai Peninsula. Gen. Tech. Rep. PNW-GTR-950. Portland, OR: U.S. Department of Agriculture, Forest Service, Pacific Northwest Research Station. 340 pp.
- Hengl, T., Mendes De Jesus, J., Heuvelink, G.B.M., Gonzalez, M.R., Kilibarda, M., Blagotí, A., Shangguan, W., Wright, M.N., Geng, X., Bauer-Marschallinger, B., Guevara, M.A., Vargas, R., Macmillan, R.A., Batjes, N.H., Leenaars, J.G.B., Ribeiro, E., Wheeler, I., Mantel, S., Kempen, B., 2016. SoilGrids250m: Global Gridded Soil Information Based on Machine Learning. PLoS One. https://doi.org/10.1371/journal.pone.0169748.
- Hinzman, L.D., Bettez, N.D., Bolton, W.R., Chapin, F.S., Dyurgerov, M.B., Fastie, C.L.,
 Griffith, B., Hollister, R.D., Hope, A., Huntington, H.P., Jensen, A.M., Jia, G.J.,
 Jorgenson, T., Kane, D.L., Klein, D.R., Kofinas, G., Lynch, A.H., Lloyd, A.H.,
 McGuire, A.D., Nelson, F.E., Oechel, W.C., Osterkamp, T.E., Racine, C.H.,
 Romanovsky, V.E., Stone, R.S., Stow, D.A., Sturm, M., Tweedie, C.E., Vourlitis, G.L.,
 Walker, M.D., Walker, D.A., Webber, P.J., Welker, J.M., Winker, K.S., Yoshikawa, K.,
 2005. Evidence and Implications of Recent climate change in northern ALASKA and
 other arctic regions. Clim. Change 72, 251–298. https://doi.org/10.1007/s10584-
- Hurtt, G.C., Chini, L., Sahajpal, R., Frolking, S., Bodirsky, B.L., Calvin, K., Doelman, J.C., Fisk, J., Fujimori, S., Klein Goldewijk, K., Hasegawa, T., Havlik, P., Heinimann, A., Humpenöder, F., Jungclaus, J., Kaplan, J.O., Kennedy, J., Krisztin, T., Lawrence, D., Lawrence, P., Ma, L., Mertz, O., Pongratz, J., Popp, A., Poulter, B., Riahi, K., Shevliakova, E., Stehfest, E., Thornton, P., Tubiello, F.N., van Vuuren, D.P., Zhang, X., 2020. Harmonization of global land use change and management for the period 850–2100 (LUH2).
- Jin, H., Huang, Y., Bense, V.F., Ma, Q., Marchenko, S.S., Shepelev, V.V., Hu, Y., Liang, S., Spektor, V.V., Jin, X., Li, X., Li, X., 2022. Permafrost Degradation and Its Hydrogeological Impacts. Water 2022 (14), 372. https://doi.org/10.3390/w14030372
- Kao, S.-C., Ashfaq, M., Naz, B. S., Uria Martinez, R., Rastogi, D., Mei, R., Jager, Y., Samu, N.M., and Sale, M.J. 2016: The Second Assessment of the Effects of Climate Change on Federal Hydropower. United States10.2172/1340431.
- Kay, A.L., Davies, H.N., Bell, V.A., Jones, R.G., 2009. Comparison of uncertainty sources for climate change impacts: flood frequency in England. Clim. Change 92, 41–63. https://doi.org/10.1007/s10584-008-9471-4.
- Lader, R., Walsh, J.E., Bhatt, U.S., Bieniek, P.A., 2017. Projections of twenty-first-century climate extremes for Alaska via dynamical downscaling and quantile mapping. J. Appl. Meteorol. Climatol. 56, 2393–2409. https://doi.org/10.1175/JAMC-D-16-0415.1.
- Lader, R., Walsh, J.E., Bhatt, U.S., Bieniek, P.A., 2020. Anticipated changes to the snow season in Alaska: elevation dependency, timing and extremes. Int. J. Climatol. 40 (1), 169–187. https://doi.org/10.1002/joc.6201.
- Lawrence, D., Slater, A., 2008. Incorporating organic soil into a global climate model. Clim. Dyn. 30, 145–160. https://doi.org/10.1007/s00382-007-0278-1.
- Liang, X., Lettenmaier, D.P., Wood, E.F., Burges, S.J., 1994. A simple hydrologically based model of land surface water and energy fluxes for general circulation models. J. Geophys. Res. 99, 14415–14428. https://doi.org/10.1029/94jd00483.
- Littell, J., McAfee, S., Hayward, G., 2018. Alaska Snowpack Response to Climate Change: Statewide Snowfall Equivalent and Snowpack Water Scenarios. Water 10 (5), 668.
- Longman, R.J., Frazier, A.G., Newman, A.J., Giambelluca, T.W., Schanzenbach, D., Kagawa-Viviani, A., Needham, H., Arnold, J.R., Clark, M.P., 2019. High-Resolution Gridded Daily Rainfall and Temperature for the Hawaiian Islands (1990–2014).
 J. Hydrometeorol. 20, 489–508. https://doi.org/10.1175/JHM-D-18-0112.1.
- Mair, A., A. G. Johnson, K. Rotzoll, and D. S. Oki, 2019: Estimated groundwater recharge from a water-budget model incorporating selected climate projections, Island of

- Maui, Hawai'i. U.S. Geological Survey Scientific Investigations Report 2019–5064. 46 pp10.3133/sir20195064.
- Maurer, E.P., Brekke, L., Pruitt, T., Thrasher, B., Long, J., Duffy, P., Dettinger, M., Cayan, D., Arnold, J., 2013. An enhanced archive facilitating climate impacts and adaptation analysis. Bull. Am. Meteorol. Soc. 95, 1011–1019. https://doi.org/ 10.1175/bams-d-13-00126.1.
- Mendoza, P.A., Clark, M.P., Mizukami, N., Newman, A.J., Barlage, M., Gutmann, E.D., Rasmussen, R.M., Rajagopalan, B., Brekke, L.D., Arnold, J.R., 2015. Effects of hydrologic model choice and calibration on the portrayal of climate change impacts. J. Hydrometeorol. 1610.1175/JHM-D-14-0104.1.
- Mizukami, N., Clark, M.P., Gutmann, E.D., Mendoza, P.A., Newman, A.J., Nijssen, B., Livneh, B., Hay, L.E., Arnold, J.R., Brekke, L.D., 2016. Implications of the methodological choices for hydrologic portrayals of climate change over the contiguous United States: statistically downscaled forcing data and hydrologic models. J. Hydrometeorol. 17, 73–98. https://doi.org/10.1175/jhm-d-14-0187.1.
- Mizukami, N., Clark, M.P., Newman, A.J., Wood, A.W., Gutmann, E.D., Nijssen, B., Rakovec, O., Samaniego, L., 2017. Towards seamless large-domain parameter estimation for hydrologic models. Water Resour. Res. 5310.1002/2017WR020401.
- Monteith, J.L., 1973. Principles of Environmental Physics. Elsevier, New York.
- Najafi, M.R., Moradkhani, H., Jung, I.W., 2011. Assessing the uncertainties of hydrologic model selection in climate change impact studies. Hydrol. Process. 25, 2814–2826. https://doi.org/10.1002/hyp.8043.
- Newman, A.J., Clark, M.P., Longman, R.J., Gilleland, E., Giambelluca, T.W., Arnold, J.R., 2019. Use of daily station observations to produce high-resolution gridded probabilistic precipitation and temperature time series for the Hawaiian Islands. J. Hydrometeorol. 20, 509–529.
- Newman, A.J., Arnold, J.R., Wood, A.W., Gutmann, E.D., 2022. A workshop on improving our methodologies of selecting earth system models for climate change impact applications. Bull. Am. Meteorol. Soc. 103 (4). E1213 E1219.
- Newman, A. J., Clark, M.P., Wood, A.W, Arnold, J.R., 2020. Probabilistic spatial meteorological estimates for Alaska and the Yukon. J. Geophys. Research: Atmospheres. 125, e2020JD03269610.1029/2020JD032696.
- Oubeidillah, A.A., Kao, S.C., Ashfaq, M., Naz, B.S., Tootle, G., 2014. A large-scale, high-resolution hydrological model parameter data set for climate change impact assessment for the conterminous US. Hydrol. Earth Syst. Sci. 18, 67–84. https://doi.org/10.5194/hess-18-67-2014.
- Panofsky, H.A., Brier, G.W., 1968. Some Applications of Statistics to Meteorology. The Pennsylvania State University, University Park, p. 224.
- Parker, W.S., 2020. Model evaluation: an adequacy-for-purpose view. Philos. Sci. 87 (3), 457–477.
- Pfeffer, W.T., Arendt, A.A., Bliss, A., Bolch, T., Cogley, J.G., Gardner, A.S., Hagen, J.-O., Hock, R., Kaser, G., Kienholz, C., Miles, E.S., Moholdt, G., Mölg, N., Paul, F., Radić, V., Rastner, P., Raup, B.H., Rich, J., Sharp, M.J., 2014. The Randolph Glacier Inventory: a globally complete inventory of glaciers. J. Glaciol. 60 (221), 537–552.
- Prudhomme, C., Davies, H., 2009. Assessing uncertainties in climate change impact analyses on the river flow regimes in the UK. Part 1: baseline climate. Clim. Change 93, 177–195. https://doi.org/10.1007/s10584-008-9464-3.
- Rakovec, O., Mizukami, N., Kumar, R., Newman, A.J., Thober, S., Wood, A.W., Clark, M. P., Samaniego, L., 2019. Diagnostic Evaluation of Large-Domain Hydrologic Models Calibrated Across the Contiguous United States. J. Geophys. Res. Atmos. 12410.1029/2019.DD030767.
- Rasmussen, R., Liu, C., Ikeda, K., Gochis, D., Yates, D., Chen, F., Tewari, M., Barlage, M., Dudhia, J., Yu, W., Miller, K., Arsenault, K., Grubišić, V., Thompson, G., Gutmann, E., 2011. High-resolution coupled climate runoff simulations of seasonal snowfall over colorado: a process study of current and warmer climate. J. Clim. 24, 3015–3048. https://doi.org/10.1175/2010jcli3985.1.
- Reclamation, 2011. West-Wide Climate Risk Assessments: Bias-Corrected and Spatially Downscaled Surface Water Projections, Technical Memorandum. 138.
- Reclamation, 2013. Downscaled CMIP3 and CMIP5 Climate Projections Release of Downscaled CMIP5 Climate Projections, Comparison with Preceding Information, and Summary of User Needs, U.S. Department of the Interior, Bureau of Reclamation, 104 p., available at http://gdo-dcp.ucllnl.org/downscaled_cmip_projections/ techmemo/downscaled_climate.pdf.
- Reclamation, 2014. Downscaled CMIP3 and CMIP5 Hydrology Projections–Release of Hydrology Projections, Comparison with Preceding Information and Summary of User Needs, U.S. Department of the Interior, Bureau of Reclamation, 110 p., available at: http://gdo-dcp.ucllnl.org/downscaled_cmip_projections/techmemo/BCSD5HydrologyMemo.pdf.
- Reclamation, 2020. Comparing Downscaled LOCA and BCSD CMIP5 Climate and Hydrology Projections Release of Downscaled LOCA CMIP5 Hydrology. https://gdo-dcp.ucllnl.org/downscaled_cmip_projections/techmemo/LOCA_BCSD_hydrology_tech_memo.pdf. Retrieved on 04 October 2021.
- Safeeq, M., Fares, A., 2012. Hydrologic response of a Hawaiian watershed to future climate change scenarios. Hydrol. Process. 26 (18), 2745–2764.
- Schär, C., Frei, C., Lüthi, D., Davies, H.C., 1996. Surrogate climate-change scenarios for regional climate models. Geophys. Res. Lett. 23 (6), 669–672.
- Schuurman, G.W., Hawkins Hoffman, C., Cole, D.N., Lawrence, D.J., Morton, J.M., Magness, D.R., Cravens, A.E., Covington, S., O'Malley, R., Fisichelli, N.A., 2020. Resist-accept-direct (RAD)-A framework for the 21st-century natural resource manager, Natural Resource Report. https://doi.org/10.36967/nrr-2283597.
- Sicart, J.E., Hock, R., Six, D., 2008. Glacier melt, air temperature, and energy balance in different climates: The Bolivian Tropics, the French Alps, and northern Sweden. J. Geophys. Res. 113 (D24).
- Simpson, I.R., McKinnon, K.A., Davenport, F.V., Tingley, M., Lehner, F., Al Fahad, A., Chen, D., 2021. Emergent constraints on the large-scale atmospheric circulation and

- regional hydroclimate: do they still work in CMIP6 and how much can they actually constrain the future? J. Clim. 34 (15), 6355–6377.
- Sun, Q. C. Mial, A. AghaKouchak, I. Mallakpour, D. Ji, and Q. Duan, 2020: Possible increased frequency of ENSO-Related Dry and Wet Conditions over some major watersheds in a warming climate. Bull. American Meteorol. Soc., 101, E409-E426, doi:10.1175/BAMS-D-18-0258.1.
- Snover, Amy, Mantua, Nathan, Littell, Jeremy, Alexander, Michael, Mcclure, Michelle, Nye, Janet, 2013. Choosing and Using Climate-Change Scenarios for Ecological-Impact Assessments and Conservation Decisions. Conserv. Biol. 27, 1147–1157. https://doi.org/10.1111/cobi.12163.
- Surfleet, C.G., Tullos, D., 2013. Uncertainty in hydrologic modelling for estimating hydrologic response due to climate change (Santiam River, Oregon). Hydrol. Process. 27 (25), 3560–3576.
- Tachikawa, T., Kaku, M., Iwasaki, A., Gesch, D.B., Oimoen, M.J., Zhang, Z., Danielson, J. J., Krieger, T., Curtis, B., Haase, J., Abrams, M., Carabajal, C., 2011. ASTER Global Digital Elevation Model Version 2 summary of validation results. http://pubs.er. usgs.gov/publication/70005960.
- Terando, A., Reidmiller, D., Hostetler, S.W., Littell, J.S., Beard Jr., T.D., Weiskopf, S.R., Belnap, J., Plumlee, G.S., 2020. Using information from global climate models to inform policymaking—The role of the U.S. Geological Survey, Open-File Report. Reston, VA. https://doi.org/10.3133/ofr20201058.
- Thompson, Laura, et al., 2021. Responding to Ecosystem Transformation: Resist, Accept, or Direct? Fisheries 46, 8–21. https://doi.org/10.1002/fsh.10506.
- Thornton, P.E., Running, S.W., 1999. An improved algorithm for estimating incident daily solar radiation from measurements of temperature, humidity, and precipitation. Agric. For. Meteorol. 93 (4), 211–228.
- Thornton, P.E., M.M. Thornton, B.W. Mayer, Y. Wei, R. Devarakonda, R.S. Vose, and R.B. Cook. 2016. Daymet: Daily Surface Weather Data on a 1-km Grid for North America, Version 3. ORNL DAAC, Oak Ridge, Tennessee, USA10.3334/ORNLDAAC/1328.
- Tokarska, K.B., Stolpe, M.B., Sippel, S., Fischer, E.M., Smith, C.J., Lehner, F., Knutti, R., 2020. Past warming trend constrains future warming in CMIP6 models. Science advances 6 (12), eaaz9549.
- Vano, J.A., Udall, B., Cayan, D.R., Overpeck, J.T., Brekke, L.D., Das, T., Hartmann, H.C., Hidalgo, H.G., Hoerling, M., McCabe, G.J., Morino, K., Webb, R.S., Werner, K.

- Lettenmaier, D.P., 2014. Understanding Uncertainties in Future Colorado River Streamflow. Bull. Am. Meteorol. Soc. 95, 59–78. https://doi.org/10.1175/bams-d-
- Vidal, J.-P., Hingray, B., Magand, C., Sauquet, E., Ducharne, A., 2016. Hierarchy of climate and hydrological uncertainties in transient low-flow projections. Hydrol. Earth Syst. Sci. 20, 3651–3672. https://doi.org/10.5194/hess-20-3651-2016.
- Walsh, J.E., Bhatt, U.S., Littell, J.S., Leonawicz, M., Lindgren, M., Kurkowski, T.A., Bieniek, P.A., Thoman, R., Gray, S., Rupp, T.S., 2018. Downscaling of climate model output for Alaskan stakeholders. Environ. Model. Softw. 110, 38–51. https://doi. org/https://doi.org/10.1016/j.envsoft.2018.03.021.
- Williamson, M.S., Thackeray, C.W., Cox, P.M., Hall, A., Huntingford, C., Nijsse, F.J., 2021. Emergent constraints on climate sensitivities. Rev. Modern Phys. 93 (2), 025004
- Wood, A.W., Leung, L.R., Sridhar, V., Lettenmaier, D.P., 2004. Hydrologic Implications of Dynamical and Statistical Approaches to Downscaling Climate Model Outputs. Clim. Change 62, 189–216. https://doi.org/10.1023/B: CLIM.0000013685.99609.9e.
- Wootten, A.M., Dixon, K.W., Adams-Smith, D.J., McPherson, R.A., 2021. Statistically downscaled precipitation sensitivity to gridded observation data and downscaling technique. Int. J. Climatol. 41 (2), 980–1001.
- Xue, L., Wang, Y., Newman, A.J., Ikeda, K., Rasmussen, R.M., Giambelluca, T.W., Longman, R.J., Monaghan, A.J., Clark, M.P., Arnold, J.R., 2020. How will rainfall change over Hawai'i in the future? High-resolution regional climate simulation of the Hawaiian Islands. Bull. Atmos. Sci. Technol. 1, 459–490. https://doi.org/ 10.1007/s42865-020-00022-5.
- Yang, Y., Pan, M., Beck, H.E., Fisher, C.K., Beighley, R.E., Kao, S.-C., Hong, Y., Wood, E. F., 2019. In Quest of calibration density and consistency in hydrologic modeling: distributed parameter calibration against streamflow characteristics. Water Resour. Res. 55 (9), 7784–7803.
- Zhang, C., Wang, Y., Hamilton, K., Lauer, A., 2016. Dynamical downscaling of the climate for the Hawaiian Islands. Part II: Projection for the late twenty-first century. J. Clim 29 (23), 8333–8354.